JOURNAL OF PROPULSION AND POWER
Vol. 25, No. 4, July–August 2009

Zero-Dimensional Time-Dependent Model of High-Pressure Ablative Capillary Discharge for Plasma Thrusters

L. Pekker*
ERC, Inc., Edwards Air Force Base, California 93524

DOI: 10.2514/1.41076

A zero-dimensional time-dependent high-pressure slab capillary discharge model is presented. The model includes a heat-transfer radiation model based on a radiation database constructed using PrismSPECT, a commercially available radiation software, to calculate the radiation heat flux output from a uniform plasma slab. Thus, unlike earlier models, this model does not use any asymptotic radiation models, but self-consistently calculates the radiation heat flux at the thin transition layer between the uniform plasma core and the ablative capillary walls. The model predicts the existence of two steady-state regimes at a given plasma temperature. The first regime occurs when the plasma is so dense that the radiation mean free path, λ_{rad}, is less than the slab gap of the capillary, D_c, that is, the case of superhigh-pressure capillary discharge. The second regime occurs when the plasma density is much lower, so that $\lambda_{\mathrm{rad}} \gg D_c$, that is, the case of moderately high plasma pressure. Both regimes converge at the small plasma temperature, and there is no steady-state solution for smaller plasma temperatures. Calculations show that the density of the plasma in the second regime may become so small that the conduction heat flux to the wall becomes larger than the radiation flux to the capillary wall, transitioning from radiation mode to thermal conduction mode. We show that in this mode the capillary discharge can still exist when local thermodynamic equilibrium is valid and the ratio of thermal pressure to magnetic pressure is greater than 1, $\beta \gg 1$. Both regimes, radiation and thermal conduction, may be attractive for thruster applications depending on specific configurations.

Nomenclature

A_a	=	mass of a neutral atom, au
A_c	=	cross-sectional area of capillary discharge
A_i	=	mass of an ion, au
A_{wall}	=	surface area of the capillary wall
a_k	=	index for type-k neutral atoms
a_0	=	Bohr radius
B	=	magnitude of magnetic field
CH	=	index for CH molecule
C_s	=	sound speed
C_α	=	carbon fraction of polyethylene molecule
cyl	=	index for cylindrical symmetry
c_p	=	specific heat at constant pressure
D_c	=	slab capillary gap
$D_{e,\mathrm{diffus}}$	=	electron diffusion coefficient
D_{tbl}	=	thickness of the transition boundary layer
E	=	magnitude of electrical field
e	=	electron charge
end	=	index denoting condition at the exit plane
F_{BBR}	=	blackbody radiation
F_{rad}	=	radiation heat flux incident on the transition boundary layer
$F_{\mathrm{rad},w}$	=	radiation heat flux incident on the capillary wall
$F_{T\text{-Cond}}$	=	conduction heat flux
f	=	gray factor
H_α	=	hydrogen fraction of polyethylene molecule
h	=	Planck constant
h_{CH}	=	enthalpy of a CH molecule to bring it from the capillary wall to the plasma volume
h_{out}	=	enthalpy of the plasma leaving the capillary per unit of volume
h_{vap}	=	specific enthalpy of evaporation
I	=	ionization potential
I_H	=	hydrogen ionization potential
ion	=	index for ionization process
i_k	=	index for type-k ions
J_{cyl}	=	total current for cylindrical capillary
J_{slab}	=	capillary discharge current per unit of slab length
K_{LPCE}	=	local plasma-chemistry equilibrium factor
K_{LTE}	=	local thermodynamic equilibrium factor
K_{VIS}	=	viscosity factor
k	=	index for type-k species
k_B	=	Boltzmann constant
L_c	=	capillary length
l	=	index for l-ionized atom
$\dot{M}$	=	rate of mass ablation
Ma	=	Mach number
M_a	=	average mass of heavy particles
M_{C}	=	carbon atom mass
M_{H}	=	hydrogen atom mass
M_i	=	ion mass
M_0	=	unit of atomic mass
m_e	=	electron mass
$\dot{N}_{\mathrm{CH}}^{\mathrm{in}}$	=	CH-molecular ablation rate
$\dot{N}_{\mathrm{CH}}^{\mathrm{out}}$	=	CH-molecular outflow through the open capillary end
$\dot{N}_e$	=	total number of electrons leaving the capillary chamber per unit time
$\dot{N}_{e,\mathrm{diffus}}$	=	outflow of electrons due to their diffusion to the capillary wall
$\dot{N}_{e\text{-imp}}^{\mathrm{ioniz}}$	=	number of electron impact ionization events per unit of time
$\dot{N}_{e,\mathrm{outflow}}$	=	outflow of electrons through the open capillary end
$\dot{N}_{3\text{-body}}^{\mathrm{recom}}$	=	number of recombination events in three-body collisions per unit of time
n	=	number density

Presented as Paper 3891 at the 39th Plasmadynamics and Laser Conference, Seattle, WA, 23–26 June 2008; received 17 September 2008; revision received 26 January 2009; accepted for publication 10 April 2009.

*Research Scientist; Leonid.Pekker.ctr@edwards.af.mil.

n_a = number density of neutral atoms
n_{CH} = mole number density of ablated molecules
n_e = electron number density
n_i = ion number density
P = pressure
$\dot{Q}_{\mathrm{outflow}}$ = rate of energy leaving the capillary through the open end
$Q_{T\text{-Cond}}$ = conduction heat flow at the transition layer
$\dot{Q}_{\mathrm{vis}}$ = heating rate due to friction forces in the viscosity boundary layer
R_c = capillary radius
recom = index for recombination process
slab = index for slab symmetry
T = plasma temperature
T_e = electron temperature
T_{wall} = temperature of the capillary wall
Tran-layer = index for the transition layer
u_d = ionization cost per ionization
V_{bound} = gas velocity at the boundary of the viscosity boundary layer
V_c = capillary chamber volume
V_{Te} = electron thermal velocity
V_{Th} = thermal velocity of heavy particles
V_x = velocity in the x direction
$v_{e,\mathrm{drift}}$ = electron drift velocity
Z = ion charge state
β = ratio of thermal pressure to magnetic pressure
Γ = parameter depending on ratio of specific heats
γ = ratio of specific heats
γ_e = nonideal factor in electron–ion collision frequency
ΔI = reduction in the ionization potential
ΔW = average energy an electron gains from the electric field E between collisions with heavy particles
ΔW_{ea} = average energy an electron gains from the electric field E between electron-neutral collisions
ΔW_{ei} = average energy an electron gains from the electric field E between electron–ion collisions
$\Delta\varepsilon_{e\langle=\rangle a}$ = average electron-neutral exchange energy due to elastic collisions
$\Delta\varepsilon_{e\langle=\rangle i}$ = average electron–ion exchange energy due to elastic collisions
$\Delta\varepsilon_{e\langle=\rangle i,a}$ = average electron exchange energy due to elastic collisions with ions and neutral atoms
$\Delta\varepsilon_{\Phi}$ = sum of ablation, dissociation, ionization, and electronic excitation energies
δ = thickness of the viscosity boundary layer
ε = internal energy
$\varepsilon_{\mathrm{CH}}$ = internal plasma energy per CH molecule
ε_e = kinetic energy per electron
ε_0 = permittivity of free space
η = viscosity coefficient
Λ_{ee} = electron–electron Coulomb logarithm
Λ_{ei} = electron–ion Coulomb logarithm
Λ_m = nonideal factor in electron–ion collision frequency
λ_D = Debye length
λ_e = electron transport mean free path
λ_{ea} = electron-neutral collision mean free path
λ_{hh} = average collision mean free path for heavy particles (neutrals and ions)
λ_{rad} = Rosseland radiation mean free path
μ_0 = permeability of free space
ν_{ea} = collision frequency between electrons and neutral atoms
ν_{ee} = electron–electron collision frequency
ν_{ei} = collision frequency between electrons and ions
ξ = three-body recombination coefficient
ρ = plasma mass density
$\dot{\rho}$ = rate of ablation mass density averaged over the cross section of the capillary
σ = electrical conductivity
σ_{ea} = electron collision cross sections with a neutral atom
σ_{eC} = electron collision cross sections with a neutral carbon atom
σ_{eH} = electron collision cross sections with a neutral hydrogen atom
σ_{ion} = ionization cross sections
σ_{SB} = the Stefan–Boltzmann constant
φ = ionization ratio
χ_e = electron thermal conductivity
Ω = de Broglie wavelength

I. Introduction

THE role of space-based systems for both commercial and government customers continues to evolve, continually providing new requirements for the development of satellite propulsion systems. One development path is toward ever-increasing power levels (tens of kilowatts) in compact, efficient thrusters. As it is very efficient (50–70% kinetic-to-electric-power ratio), high-pressure (5×10^6–5×10^8 Pa) ablative capillary discharge is a good candidate for high-power plasma thrusters. The first paper to discuss the use of ablative capillary discharge for propulsion was published in the United States in 1982 [1]. In it, the authors introduced their concept of the pulsed electrothermal thruster; this group later built and tested such devices [2,3]. In recent theoretical papers [4–9], the authors continued to explore the application of such discharges to electrothermal capillary thrusters.

A schematic of a slab capillary discharge thruster is shown in Fig. 1. The discharge maintains a resistive arc through a narrow insulating capillary by the continual ablation of an injected mass or, more commonly, the capillary wall material, as shown in Fig. 1. The ablative capillary discharge can be described via a three-layer configuration. The outermost layer is a solid wall, usually some form of polyethylene, occasionally Teflon® or some other insulating material. Material from the wall is evaporated, entering the thin transition boundary layer, where it is dissociated, ionized, and heated to plasma temperature. The innermost layer is the plasma core. The closed end of the capillary (left side of Fig. 1) is one electrode; the other electrode (right side of Fig. 1) is an open end through which the plasma can flow and expand. The polarity has no appreciable effect on discharge operation. Ohmic heating is responsible for heating, ionization, ablation, and radiation. In the model, a sonic condition ($Ma = 1$ in Fig. 1) is assumed to exist at the open end of the capillary.

In terms of plasma propulsion concepts, the capillary plasma thruster must satisfy two main conditions. First, the capillary plasma should be in a local thermodynamic equilibrium (LTE), indicating that all sorts of particles, electrons, ions, and neutrals have the same temperature. Then, the electrical current will heat both the electrons and the heavy particles (i.e., not only the electrons), thus providing high thrust per watt. Second, as it is well known, pinching the capillary discharge leads to a formation of a narrow plasma core region with a high electron temperature and a large, relatively cold peripheral plasma region. This also decreases the efficiency of the capillary thruster, because only a small amount of input discharge

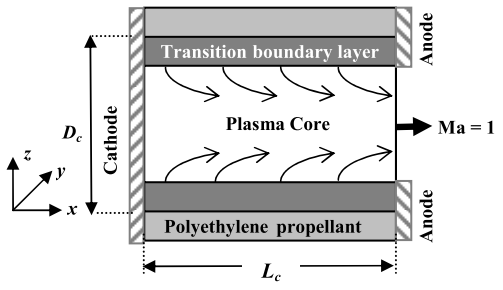

Fig. 1 Schematic (not to scale) of slab capillary discharge operation; (z, x) cross section is shown.

energy is transferred to the heavy particles and almost all of the input energy is transferred to the electrons. To minimize the pinching of the capillary discharge, the ratio of the thermal pressure to the magnetic pressure, β, in the capillary plasma thruster should be greater than unity.

The ablative capillary discharges that have been previously studied as potential electrothermal and electrothermochemical gun devices by various investigators since the mid-1980s (see [10–20] and the references therein) satisfy both of these conditions well. These studies investigated the dynamics of high-pressure ablative plasma discharges; they gave pressures in a range of 0.1–1 GPa and temperatures of the order of 1–3 eV.

In all theoretical zero- and one-dimensional models of ablative capillary discharges [4–16,19,20], the thickness of the transition layer, Fig. 1, is assumed to be negligibly small compared with the inner capillary radius and the radial distributions of plasma parameters in the plasma core are assumed to be uniform. This assumption is based on the premise that the radial radiation heat transfer across the capillary chamber is so strong that it flattens the temperature and density distributions across the plasma core, leading to a very thin transition layer. As mentioned in [11], the strong plasma convection that can develop in the capillary discharge can also lead to the flattening of the capillary discharge parameters in the plasma core and thin boundary layer. Unfortunately, there exists no model of the ablative capillary discharge that would verify this premise. The main challenge for constructing such a model is a comprehensive description of the radial heat transfer in the capillary discharge.

It is worth noting that, in other types of capillary discharges operating in a nonablation regime with much faster pulses, a lower pressure, a high electron temperature in the plasma cores (no LTE), and $\beta < 1$, the plasma density is usually so small that thermal conduction, not radiation, is responsible for the heat transfer across the capillary and the creation of the nonflat radial plasma density and temperature distributions [21–24]. These discharges have been used as x-ray radiation sources in spectroscopy and lithography for wakefield acceleration and ultra-intense laser guiding. Unlike in ablative capillary discharges, in these plasma sources capillary chambers are filled by a gas and the capillary walls are made from a ceramic material preventing large ablation. However, as it will be shown in this work, ablative capillary discharges may also be operated in a low-pressure regime with thermal conduction heat larger than radiative heat (as in nonablative capillary plasma sources), but with plasma in LTE and $\beta > 1$, as desired for propulsion applications.

The first comprehensive zero-dimensional analytical model of ablative capillary discharges was developed by Loeb and Kaplan [11]. By balancing ohmic heating via radiation losses, wall ablation, and plasma outflow, they obtained scaling laws for the plasma temperature, pressure, wall ablation rate, and other parameters of the capillary discharge as functions of the current, capillary radius, and capillary length. Some key assumptions made in this model include the following: 1) plasma radiation is modeled as blackbody radiation; 2) the radiation flux incoming to the boundary layer (Fig. 1) ablates the wall material, dissociates, ionizes, and heats ablated vapor to the plasma conditions, and no heat losses occur in the bulk wall; 3) the plasma is fully ionized; and 4) when calculating the plasma enthalpy, the energy cost of ionization is neglected. The last assumption can be a serious error, because, for example, carbon ions can be twice and even three times ionized; therefore, the contribution of the ionization cost to the total plasma enthalpy can be very large, causing the dependence of enthalpy on temperature to be very different than assumed in the model [11]. These simplifications allowed Loeb and Kaplan to obtain analytical solutions to the scaling laws, a significant progress at that time. However, these scaling laws are somewhat questionable, due to the degree of approximations. In further works [4–9,12–16,19,20], the Saha equation is used to more accurately calculate the plasma composition and enthalpy of the plasma.

In the time-dependent Gilligan–Mohanti zero-dimensional model [12], the rate of mass ablation $\dot{M}$ is determined by converting the radiation incident on the solid wall:

$$\dot{M} \cdot h_{\text{vap}} = F_{\text{rad},w} \cdot A_{\text{wall}} \tag{1}$$

Gilligan and Mohanti assume $F_{\text{rad},w}$ to be a fraction f (the gray factor) of the blackbody radiation leaving the arc:

$$F_{\text{rad},w} = f \cdot \sigma_{\text{SB}} \cdot T^4 \tag{2}$$

Assuming local thermodynamic equilibrium and using the Saha equation, Gilligan and Mohanti calculate the internal energy of the plasma, the resistivity, and other thermodynamic parameters. To get agreement with the experiments, they are required assume that only a small fraction ($f \ll 1$) of the plasma radiation reaches the wall. Thus, this model demonstrates the obvious fact that only a small fraction of the energy in the discharge is actually spent on evaporating the wall and that the main part of the input energy is spent on dissociating, ionizing, and heating the ablated material to plasma temperature.

In one-dimensional models (see [13–17,19,20] and the references therein), the authors calculate the plasma composition, resistivity, temperature, and other plasma parameters along the capillary discharge by using different levels of approximations and simplifications. However, all these models assume LTE in the plasma layer and $\beta \gg 1$ and no heat losses in the bulk of the capillary walls. In [13–16,19,20], the authors calculate the ablation mass density rate $\dot{\rho}$ averaged over the cross section of the capillary as

$$\dot{\rho} = \frac{2 \cdot f \cdot \sigma_{\text{SB}} \cdot T^4 / R_c}{\varepsilon + P/\rho} \tag{3}$$

where $f \cdot \sigma_{\text{SB}} \cdot T^4$ is the radiation heat flux incoming to the transition boundary layer, whereas Raja et al. [17] have used basically Eqs. (1) and (2).

In these models, the gray factor ranges between 0.6–0.85 and 0.05–0.1 to fit the experimental data depending on whether the authors consider the radiation flux either at the plasma-transition interface [13–16,19,20], Eq. (3), or at the ablative surface [17], Eqs. (1) and (2). This indicates that plasma radiation in experiments [13,15–17] cannot be described by a pure blackbody radiation approximation, and the Rosseland radiation mean free path λ_{rad} is larger than the capillary radius.

In [6–9], the authors modeled electrothermal pulsed plasma thrusters using a different (nonblackbody-type) radiation model, a volumetric bremsstrahlung (free–free) radiation model, and self-consistently calculated the parameters of the capillary discharge; no gray factor was used in the models. In their radiation models, they completely ignored the recombination (free–free) and inline (bound–bound) radiation. However, our calculation of the radiation balance using PrismSPECT radiation software[†] shows that the free–bound and bound–bound electron transitions are the main contributors to the total radiation balance in high-pressure capillary discharge. Thus, using only bremsstrahlung radiation in modeling high-pressure capillary discharge is questionable.

Using a zero-dimensional ablative capillary discharge model [4], the authors have shown that steady-state ablative capillary discharge may in fact exist in two regimes. In the first regime, the superhigh-pressure (SHP) regime, the plasma density is assumed to be extremely high so that the plasma is opaque to its own radiation; in this case, a blackbody radiation approximation is applied. This regime corresponds to the previously developed models with the gray factor equal to 1. In the second regime, the moderately high-pressure (MHP) regime, the plasma density in the plasma core is assumed to be much smaller so that the plasma is completely transparent to its own radiation, but the transition layer is assumed to be opaque to the plasma radiation and to absorb all incoming radiation. In this regime, the radiation model includes bremsstrahlung (free–free) radiation and recombination (free–bound) radiation; the bound–bound radiation is ignored. It should be stressed that the last assumption excludes the applicability of this regime to the case of

[†]Prism Computational Sciences, Inc., 455 Science Drive, Suite 140, Madison, WI 53711.

partially ionized plasma and multicharged fully ionized plasma, for which the line radiation (bound–bound radiation) can be much larger than the continuum radiation. However, the results obtained in this moderately high-pressure regime are, probably, a valid guideline for the case of pure hydrogen (a propellant of choice for high-performance propulsion), wherein hydrogen plasma is assumed to be fully ionized and bound-bound radiation is absent. The prospects of ablative capillary discharges for propulsive applications are also discussed in this paper.

Thus, all previously developed models of ablative capillary discharges either consider the asymptotic radiation cases, blackbody and volumetric radiation regimes, or use blackbody radiation with a gray factor to obtain agreement with the experiments; the experiments, probably, correspond to intermediate regimes between the blackbody and volumetric regimes.

In a recent zero-dimensional high-pressure (5×10^6–5×10^8 Pa) capillary discharge model [5], the authors used a radiation heat-transfer model based on a radiation database. This database was constructed using PrismSPECT, a commercially available radiation software, to calculate the radiation spectrum output from a uniform plasma sphere. The authors applied the spectra obtained from a plasma sphere with radius R_c to a cylindrical capillary with the same radius, because PrismSPECT does not support cylindrical symmetry. Although such a method is not consistent, it allowed a self-consistent calculation of the radiation transport for the first time, without introducing a gray factor, f, Eqs. (2) and (3). Thus, unlike previous models, this model [5] did not use any "asymptotic" radiation models, but self-consistently calculated the radiation heat flux at the transition layer.

The present paper describes the high-pressure capillary discharge model [5] in detail and extends it to the case of slab geometry supported by PrismSPECT. An analysis of the assumptions made in the model is given in Sec. II, the description of the model and numerical results are presented in Secs. III and IV, respectively, and the conclusions are in Sec. V.

II. Model Assumptions

The following assumptions are made in the model: 1) the temperatures of electrons and heavy particles (ions and neutrals) are equal, that is, the LTE condition is achieved; 2) plasma composition can be calculated using the Saha equation, that is, local plasma-chemistry equilibrium is achieved; 3) heating of the plasma by the viscosity drag force is small and can be omitted; 4) magnetic pressure is much smaller than thermal pressure, that is, $\beta \gg 1$; and 5) the conduction heat flux is much smaller than the radiation flux and can be ignored. These assumptions are described in order in Secs. II.A–II.E, respectively. Plasma composition and geometry assumptions are discussed in detail in Sec. II.F.

A. Local Thermodynamic Equilibrium Factor (LTE Factor)

Because for typical ablative high-pressure capillary discharge, the mean free paths for neutral–neutral and neutral–ion collisions are much smaller than the capillary radius (capillary slab gap D_c in slab geometry), the ions and neutrals have the same local temperature, that is, they are in local thermodynamic equilibrium.

In the plasma capillary core region, Fig. 1, where the plasma is usually almost fully ionized, or at least well ionized, the electron–ion collisions play a major role in determining local thermodynamic equilibrium between electrons and heavy particles (ions and neutrals). In the electron–ion collision process, the colliding particles lose or gain some energy from each other; the average exchange energy between the particles due to elastic collisions can be estimated as

$$\Delta\varepsilon_{e\langle=\rangle i} \approx k_B \cdot T \cdot \left(\frac{2 \cdot m_e}{M_i}\right) \tag{4}$$

The average energy ΔW_{ei} that an electron gains from the electric field E between collisions is

$$\Delta W_{ei} = \frac{e \cdot E \cdot v_{e,\text{drift}}}{\nu_{ei}} \tag{5}$$

where ν_{ei} is the electron–ion collision frequency, and $v_{e,\text{drift}}$ is the electron drift velocity:

$$v_{e,\text{drift}} = \frac{e \cdot E}{m_e \cdot \nu_{ei}} \tag{6}$$

Substituting Eq. (6) into Eq. (5), we obtain

$$\Delta W_{ei} = \frac{e^2 \cdot E^2}{m_e \cdot \nu_{ei}^2} = 1.18 \times 10^{-14} \cdot \frac{E^2\ [\text{V/m}] \cdot T_e^3\ [\text{eV}]}{\Lambda_{ei}^2 \cdot Z^4 \cdot n_i^2\ [\text{m}^{-3}]} \quad \text{in [eV]} \tag{7}$$

In Eq. (7), we have used this expression for the electron–ion elastic collision frequency ν_{ei}:

$$\nu_{ei} = 3.94 \times 10^{-12} \cdot \frac{\Lambda_{ei} \cdot Z^2 \cdot n_i\ [\text{m}^{-3}]}{T_e^{3/2}\ [\text{eV}]} \quad \text{in [s}^{-1}\text{]} \tag{8}$$

taken from the Naval Research Laboratory brochure.[‡] Here, $n_e = Z \cdot n_i$ is the electron number density (the plasma is assumed to be quasi neutral). Now let us introduce the LTE factor, K_{LTE}, as the ratio of $\Delta\varepsilon_{e\Leftrightarrow iv}$, Eq. (4), to ΔW_{ei}, Eq. (7):

$$K_{\text{LTE}} = \frac{\Delta\varepsilon_{e\Leftrightarrow i}}{\Delta W_{ei}} = 9.5 \times 10^{-38} \cdot \frac{n_i^2\ [\text{m}^{-3}] \cdot Z^4 \cdot \Lambda_{ei}^2}{A_i \cdot T^2\ [\text{eV}] \cdot E^2\ [\text{V/m}]} \tag{9}$$

where we have substituted T for T_e in Eq. (7) and $M_0 \cdot A_i$ for M_i in Eq. (4). When this factor is large, the electron–ion collision exchange energy is larger than the average energy that the electron gains from the electric field between collisions, that is, local thermodynamic equilibrium is achieved; the electron temperature is equal to the temperature of heavy particles T. When $K_{\text{LTE}} < 1$, the electron–ion collision exchange energy is smaller than the average energy that the electron gains from the electric field between collisions, that is, there is no local thermodynamic equilibrium. In this case, the electron temperature is higher than the temperature of heavy particles and is determined by balancing the energy that the electron gains from the electrical field with that transferred to ions. Thus, substituting T_e instead of T into Eq. (4) and setting this equation equal to Eq. (7), we obtain the following estimate for the electron temperature:

$$T_e\ [\text{eV}] \approx 3 \times 10^{-19} \cdot \frac{n_i\ [\text{m}^{-3}] \cdot Z^2 \cdot \Lambda_{ei}}{A_i^{1/2} \cdot E\ [\text{V/m}]} \tag{10}$$

Obviously, the electron temperature T_e obtained this way forces K_{LTE} to equal 1. For the case of multi-ion plasma composition, Eq. (9) can be rewritten as

$$K_{\text{LTE}} = 9.5 \times 10^{-38} \cdot \frac{\Lambda_{ei}^2}{T^2\ [\text{eV}] \cdot E^2\ [\text{V/m}]} \cdot \left(\sum_k \frac{n_{i_k} \cdot Z_k^2}{A_{i_k}}\right) \cdot \left(\sum_k Z_k^2 \cdot n_{i_k}\right) \tag{11}$$

where index k corresponds to the ions of type k and densities are in m^{-3}. In this equation, we have averaged $1/A_i$ with the weight function equal to the collision frequency of electrons with a given type of ions:

$$\frac{1}{A_i} = \frac{\sum_k (\nu_{ei_k} \cdot (A_{i_k})^{-1})}{\sum_k \nu_{ei_k}} \tag{12}$$

substituted

$$\nu_{ei} = \sum_k \nu_{ei_k} = \frac{3.94 \times 10^{-12}}{T_e^{3/2}\ [\text{eV}]} \cdot \Lambda_{ei} \cdot \sum_k Z_k^2 \cdot n_{i_k}\ [\text{m}^{-3}] \tag{13}$$

[‡]NRL Plasma Formulary, Naval Research Laboratory, Washington, DC 20375-5320.

and, because the Coulomb logarithms for all sorts of ions are practically the same, taken Λ_{ei} outside the brackets.

Now let us consider the LTE factor in the transition boundary layer, Fig. 1, where the "plasma" temperature is small, about 0.3–1 eV, the gas is weakly ionized, and, therefore, the electron-neutral collisions play the main role in the determination of the LTE in this layer. For the electron-neutral collision process the average exchange energy between neutrals and electrons is given by Eq. (4), where we have to substitute index a for index i:

$$\Delta\varepsilon_{e\langle=\rangle a} \approx T \cdot k \cdot \left(\frac{2 \cdot m_e}{M_0}\right) \cdot \frac{1}{A_a}, \quad \frac{1}{A_a} = \frac{\sum\limits_k \left(\frac{\nu_{ea_k}}{A_{a_k}}\right)}{\sum\limits_k \nu_{ea_k}} = \frac{\sum\limits_k \left(\frac{\sigma_{ea_k} \cdot n_{a_k}}{A_{a_k}}\right)}{\sum\limits_k (\sigma_{ea_k} \cdot n_{a_k})} \tag{14}$$

Here, n_{a_k} and σ_{ea_k} are the number density and the electron-neutral collision cross sections for type-k neutral atoms. Substituting into Eqs. (5) and (6) the electron-neutral collision frequency ν_{ea_k} instead of the electron–ion collision frequency ν_{ei},

$$\nu_{ea} = \sum_k \nu_{ea_k} = V_{Te} \cdot \sum_k \left(\frac{1}{\lambda_{ea_k}}\right) = 6.21 \times 10^3 \cdot \sqrt{T_e\ [\mathrm{K}]} \cdot \sum_k (n_{a_k}\ [\mathrm{m}^{-3}] \cdot \sigma_{ea_k}[\mathrm{m}^2]) \tag{15}$$

where we have used an expression for electron thermal velocity V_{Te},

$$V_{Te} = \left(\frac{8 \cdot k_B \cdot T_e}{\pi \cdot m_e}\right) = 6.21 \times 10^3 \cdot \sqrt{T_e\ [\mathrm{K}]} \tag{16}$$

we obtain the average energy ΔW_{ea} that an electron gains from the electric field E between collisions:

$$\Delta W_{ea} = \frac{e^2 \cdot E^2}{m_e \cdot \nu_{ea}^2} = \frac{7.3 \times 10^{-16} \cdot E^2}{(\sum\limits_k n_{a_k})^2 \cdot T} \cdot \left(\sum_k \left[\frac{n_{a_k}}{(\sum\limits_k n_{a_k})} \cdot \sigma_{ea_k}\right]\right)^{-2} \tag{17}$$

Dividing $\Delta\varepsilon_{e\Leftrightarrow a}$ by ΔW_{ea} and introducing the total pressure in the transition layer as

$$P = k_B \cdot T \cdot \sum_k n_{a_k}$$

(here we have neglected the small electron pressure in the transition layer), we obtain

$$K_{\mathrm{LTE}} = 1.07 \times 10^{35} \cdot \frac{P^2}{E^2} \cdot \left(\sum_k (n_{a_k} \cdot \sigma_{ea_k})\right) \cdot \frac{\sum\limits_k (n_{a_k} \cdot \sigma_{ea_k}) \cdot \sum\limits_k \left(\frac{\sigma_{ea_k} \cdot n_{a_k}}{A_{a_k}}\right)}{(\sum\limits_k n_{a_k})^2} \tag{18}$$

where P is in pascals, E is in volts/meter, n_{a_k} is in m^{-3}, and σ_{ea_k} is in meters squared. As one can see, K_{LTE} in the transition layers is independent of the electron temperature; here we have assumed that the electron-neutral elastic cross sections are independent of the electron temperature, a fair assumption for capillary discharges.

In our capillary discharge model, we consider the C_4H_9 polyethylene capillary wall composition. Assuming that the gas in the transition layer is fully dissociated and using the electron-neutral collision cross sections [13],

$$\sigma_{eC} = 2.64 \times 10^{-19}\ [\mathrm{m}^2] \quad \text{and} \quad \sigma_{eH} = 1.49 \times 10^{-19}\ [\mathrm{m}^2]$$

we obtain

$$K_{\mathrm{LTE,C_4H_9}}^{\text{Tran-layer}} = 2.2 \times 10^{-3} \cdot (P^2/E^2) \tag{19}$$

where P is in pascals and E is in volts/meter. Thus, if the LTE factors introduced by Eqs. (11) and (19) are much larger than 1, local thermodynamic equilibrium in the capillary discharge is achieved.

It should be stressed that, for the case of the medium ionized plasma core region, the electron-neutral collisions also must be taken into account in calculating the LTE factor. Thus, Eqs. (4–6) can be rewritten as

$$\Delta\varepsilon_{e\langle=\rangle i,a} \approx k_B \cdot T \cdot \left(\frac{2 \cdot m_e}{M_0}\right) \cdot \frac{\sum\limits_k (\nu_{ei_k} \cdot (A_{i_k})^{-1}) + \sum\limits_l (\nu_{ea_l} \cdot (A_{a_l})^{-1})}{\sum\limits_k \nu_{ei_k} + \sum\limits_l \nu_{ea_l}} \tag{20}$$

$$\Delta W = \frac{e \cdot E \cdot v_{e,\mathrm{drift}}}{\sum\limits_k \nu_{ei_k} + \sum\limits_l \nu_{ea_l}} \tag{21}$$

$$v_{e,\mathrm{drift}} = \frac{e \cdot E}{m_e \cdot (\sum\limits_k \nu_{ei_k} + \sum\limits_l \nu_{ea_l})} \tag{22}$$

where collision frequencies are given by Eqs. (13) and (15). Dividing $\Delta\varepsilon_{e\Leftrightarrow i,a}$, Eq. (20), by ΔW, Eq. (21), we obtain an expression for the LTE factor for the case of the moderately ionized plasma core:

$$K_{\mathrm{LTE}_{e\Leftrightarrow i,a}} \approx k_B \cdot T \cdot \left(\frac{2 \cdot m_e^2}{e^2 \cdot E^2 \cdot M_0}\right) \cdot m_e \cdot \left(\sum_k \nu_{ei_k} + \sum_l \nu_{ea_l}\right) \cdot \left[\sum_k (\nu_{ei_k} \cdot (A_{i_k})^{-1}) + \sum_l (\nu_{ea_l} \cdot (A_{a_l})^{-1})\right] \tag{23}$$

As one can see, in our calculations of the LTE factor we have ignored inelastic collisions, assuming that inelastic collisions are less important than elastic collisions. However, this is not always the case; the inelastic collisions can play an important role in the determination of the electron temperature. Because the inelastic collisions lead to a decrease in ΔW (electrons are losing their energy inelasticity) while the energy transferred to the heavy particles in these collisions, ΔE, is about the same as in elastic collisions, we may conclude that Eqs. (9), (19), and (23) underestimate the LTE factor.

In our model we have used Eq. (23) to calculate the LTE factor, verifying the applicability of the LTE approximation used in the model. It should be stressed that the LTE approximation was used in all previously developed models [4–17,19,20] but without clear justification.

B. Local Plasma-Chemistry Equilibrium (LPCE Factor)

Let us investigate whether local ionization equilibrium in the plasma core region of high-pressure capillary discharges is achieved. Assuming LTE in the plasma core region (the electron temperature is equal to the local temperature of heavy particles, neutrals and ions; see Sec. II.A), the number of electron impact ionization events and the number of recombination events in three-body collisions ($i + e + e \rightarrow n + e + h\nu$) in the capillary plasma core region, Fig. 1, per unit of time can be estimated as

$$\dot{N}_{e\text{-imp}}^{\text{ioniz}} = 8 \cdot \sqrt{\pi} \cdot n_e \cdot n_a \cdot V_c \cdot a_0^2 \cdot \left(\frac{I_H}{I}\right)^2 \cdot \left(\frac{I}{k_B \cdot T}\right) \cdot \sqrt{\frac{2 \cdot k_B \cdot T}{m_e}} \cdot \int_{\frac{I}{k_B \cdot T}}^{\infty} \exp(-x) \cdot \left(x - \frac{I}{k_B \cdot T}\right) \cdot \frac{dx}{x} \tag{24}$$

$$\dot{N}_{\text{3-body}}^{\text{recom}} = \xi \cdot n_e^3 \cdot V_c \tag{25}$$

where $\xi = 8.75 \times 10^{-39} \cdot \mathrm{T[eV]}^{-9/2}$ is the three-body recombination coefficient [25]. In Eq. (24), we have used the Thomson approximation for the ionization cross section [25],

$$\sigma_{\mathrm{ion}}(\varepsilon_e) = 4 \cdot \pi \cdot a_0^2 \cdot \left(\frac{I_H}{\varepsilon_e}\right)^2 \cdot \left(\frac{\varepsilon_e - I}{I}\right) \tag{26}$$

and assumed the Maxwell electron distribution function. Because the characteristic plasma temperature in high-pressure capillary discharges are usually much smaller than ionization potential, $T \ll I$, Eq. (24) can be reduced to the following form:

$$\dot{N}_{e\text{-imp}}^{\text{ioniz}} = 3.97 \times 10^{-20} \cdot n_e \cdot n_a \cdot V_c \cdot \left(\frac{I_H}{I}\right)^2 \cdot \left(\frac{2 \cdot k_B \cdot T}{m_e}\right)^{1/2} \cdot \exp\left(-\frac{I}{k_B \cdot T}\right) \tag{27}$$

For the case of multi-atom composition, Eq. (27) can be rewritten as

$$\dot{N}_{e\text{-imp}}^{\text{ioniz}} = 3.97 \times 10^{-20} \cdot n_e \cdot \left(\frac{2 \cdot k_B \cdot T}{m_e}\right)^{1/2} \cdot V_c \cdot \sum_k \left[n_{a_k} \cdot \left(\frac{I_H}{I_k}\right)^2 \cdot \exp\left(-\frac{I_k}{k_B \cdot T}\right)\right] \tag{28}$$

where index k corresponds to the neutrals of type k.

The outflow of electrons through the open capillary end and their diffusion to the capillary wall can be estimated as

$$\dot{N}_{e,\text{outflow}} = n_e \cdot C_s \cdot A_c \tag{29}$$

$$\dot{N}_{e,\text{diffus}} = D_{e,\text{diffus}} \cdot \frac{n_e}{R_c} \cdot A_{\text{wall}} = \sqrt{\frac{2 \cdot k_B \cdot T}{m_e}} \cdot \lambda_e \cdot \frac{n_e}{R_c} \cdot A_{\text{wall}} \tag{30}$$

where

$$C_s \approx \sqrt{\frac{\gamma \cdot P}{\rho}} = \sqrt{\frac{\gamma \cdot (n_i + n_a + n_e) \cdot k_B \cdot T}{(n_i + n_a) \cdot M_a}} \tag{31}$$

is the sound speed at the capillary open end (sonic condition, Fig. 1). (In the case of slab geometry, one-half times the slab gap D_c has to be used instead of R_c.)

When the rates of recombination and ionization events, Eq. (25) and (28), are much larger than the number of electrons leaving the capillary chamber per unit of time,

$$\dot{N}_e = \dot{N}_{e,\text{diffus}} + \dot{N}_{e,\text{outflow}} \tag{32}$$

we may conclude that local ionization equilibrium is achieved, that is, the plasma composition is determined by balancing the ionization and recombination processes, resulting in Saha equilibrium. Thus, when both LPCE factors,

$$K_{\text{LPCE,ion}} = \frac{\dot{N}_{e\text{-imp}}^{\text{ioniz}}}{\dot{N}_e} = \frac{3.97 \times 10^{-20} \cdot V_c \cdot \sum_k n_{a_k} \cdot (\frac{I_H}{I_k})^2 \cdot \exp(-\frac{I_k}{T})}{1.69 \times 10^{-6} \cdot \frac{C_s \cdot A_c}{\sqrt{T}} + 2.3 \times 10^{17} \cdot \frac{A_{\text{wall}} \cdot T^2}{R_c \cdot \Lambda_{ee} \cdot n_e}} \tag{33}$$

and

$$K_{\text{LPCE,recom}} = \frac{\dot{N}_{3\text{-body}}^{\text{recom}}}{\dot{N}_e} = \frac{1.3 \times 10^{-44} \cdot T^{-5} \cdot n_e^2 \cdot V_c}{1.69 \times 10^{-6} \cdot \frac{C_s \cdot A_c}{\sqrt{T}} + 2.3 \times 10^{17} \cdot \frac{A_{\text{wall}} \cdot T^2}{R_c \cdot \Lambda_{ee} \cdot n_e}} \tag{34}$$

are much larger than 1, local ionization equilibrium is achieved. Here we have estimated λ_e [25] as

$$\lambda_e \approx 2.3 \times 10^{17} \cdot \frac{T^2}{\Lambda_{ee} \cdot n_e} \tag{35}$$

In Eqs. (33–35), I, I_{H}, and T are in electron volts.

It is worth noting that in the transition layer the photo-ionization processes can be more important than the electron impact ionization process due to the absorption of the large photon flux escaping from the hot plasma core region, Fig. 1, leading to an increase in the plasma temperature in this layer and a larger plasma density than that calculated by the Saha formula; in addition, the dissociative recombination process ($AB^+ + e \rightarrow A^* + B$) and impact-three-body recombination process with participation of a neutral as a third body ($i + e + a \rightarrow a + n + h\nu$) can also be more important than the $i + e + e \rightarrow n + e$ recombination process because the plasma in this region is weakly ionized.

C. Heating of the Plasma by the Viscosity Drag Force (VIS Factor)

Let us estimate plasma heating by the viscosity drag force. We can estimate the thickness of the viscosity boundary layer using the momentum equation for a quasi-stationary capillary discharge, Fig. 2,

$$\rho \cdot V_x \frac{\partial V_x}{\partial x} = -\frac{\partial P}{\partial x} - \eta \cdot \frac{\partial^2 V_x}{\partial z^2} \tag{36}$$

by setting the viscosity term equal to the left-hand term of this equation:

$$\rho \cdot V_{\text{bound}} \cdot \frac{V_{\text{bound}}}{L_c} \approx \eta \cdot \frac{V_{\text{bound}}}{\delta^2} = > \delta = \sqrt{\frac{L_c \cdot \eta}{\rho \cdot V_{\text{bound}}}} \tag{37}$$

The heating of the plasma due to friction forces in the viscosity boundary layer can be estimated as

$$\dot{Q}_{\text{visc}} \approx A_{\text{wall}} \cdot \delta \cdot \eta \cdot \frac{V_{\text{bound}}}{\delta^2} \cdot V_{\text{bound}} = A_{\text{wall}} \cdot \sqrt{\frac{\eta \cdot \rho}{L_c}} \cdot V_{\text{bound}}^{5/2} \tag{38}$$

Substituting $\eta \approx \rho \cdot V_{\text{Th}} \cdot \lambda_{hh}$ into Eq. (38), where V_{Th} and l_{hh} are the averaged thermal velocity and collision mean free path for heavy particles (neutrals and ions) in the viscosity boundary layer, we obtain

$$\dot{Q}_{\text{visc}} = A_{\text{wall}} \cdot \rho \cdot \sqrt{\frac{V_{\text{Th}} \cdot \lambda_{hh}}{L_c}} \cdot V_{\text{bound}}^{5/2} \tag{39}$$

Let us estimate the rate of energy leaving the capillary through the open end, Fig. 1, as

$$\dot{Q}_{\text{outflow}} = A_c \cdot C_s \cdot h_{\text{out}} \approx A_c \cdot C_s \cdot (n_i \cdot u_d + c_p \cdot k_B \cdot T \cdot (n_a + Z \cdot n_i + n_i)) \tag{40}$$

Let us introduce the viscosity factor (VIS factor) as the ratio of the viscosity plasma-heating rate, Eq. (39), to the outgoing energy rate, Eq. (40),

$$K_{\text{VIS}} = \frac{A_{\text{wall}} \cdot \rho \cdot V_{\text{bound}}^{5/2}}{A_c \cdot C_s \cdot (n_i \cdot u_d + c_p \cdot k_B \cdot T \cdot (n_a + Z \cdot n_e + n_i))} \cdot \sqrt{\frac{V_{\text{Th}} \cdot \lambda_{hh}}{L_c}} \tag{41}$$

If the K_{VIS} factor is small, then the heating of the plasma by the viscosity drag forces is small compared with the rate at which energy is leaving the capillary and can be neglected.

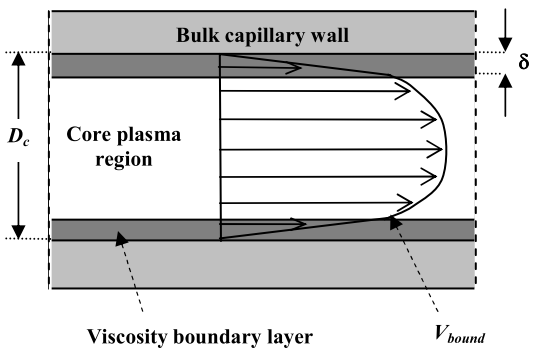

Fig. 2 Schematic radial distribution of longitudinal plasma velocity in the capillary.

D. Ratio of Thermal Pressure to Magnetic Pressure (β Factor)

The magnetic fields in slab and cylindrical geometries can be estimated as

$$B[T] = \frac{\mu_0 \cdot J_{\text{slab}}\ [\text{A/m}]}{2} \quad \text{and} \quad B[T] = \frac{\mu_0 \cdot J_{\text{cyl}}\ [\text{A}]}{2 \cdot \pi \cdot R_c\ [\text{m}]} \tag{42}$$

where J_{slab} is the total capillary current per unit of slab length along the y axis, Fig. 1, and J_{cyl} is the total current for cylindrical capillary, and μ_0 is the magnetic free-space permeability. Substituting Eqs. (42) into the equation for β,

$$\beta = 8 \cdot \pi \times 10^{-7} \cdot \frac{P\ [\text{Pa}]}{(B[T])^2}$$

we obtain

$$\beta_{\text{slab}} = \frac{2 \cdot 10^7}{\pi} \cdot \frac{P\ [\text{Pa}]}{(J_{\text{slab}}\ [\text{A/m}])^2} \quad \text{and}$$
$$\beta_{\text{cyl}} = 2 \cdot \pi \times 10^7 \cdot \frac{(R_c\ [\text{m}])^2 \cdot P\ [\text{Pa}]}{(J_{\text{cyl}}\ [\text{A}])^2} \tag{43}$$

In the model, we calculate β, validating the model assumption of $\beta \gg 1$.

E. Ratio of Thermal Conduction to Radiation Heat Transfer (COND Factor)

One of the problems in zero-dimensional modeling of the capillary discharge is to accurately estimate the conduction heat transfer to the capillary wall or to the transition layer, because the thermal conduction heat-transfer coefficient changes dramatically with the plasma-gas temperature, pressure, and plasma composition. However, in our model we estimate the radial conduction heat flux at the outer boundary of the transition layer, Fig. 1, as

$$F_{T\text{-Cond}} \approx 2 \cdot \chi_e \cdot \frac{T - T_{\text{wall}}}{D_c} \tag{44}$$

where

$$\chi_e = \frac{5 \cdot k_B^2 \cdot T \cdot n_e}{2 \cdot m_e \cdot \nu_{ee}} \quad \text{and} \quad \nu_{ee} = 3.6 \times 10^{-6} \cdot \frac{n_e\ [\text{m}^{-3}] \cdot \Lambda_{ee}}{(T\ [\text{K}])^{3/2}} \tag{45}$$

are the electron thermal conductivity [25] and the electron–electron collision frequency[‡]; in the case of cylindrical geometry, we have to substitute $2 \cdot R_c$ for D_c. Substituting ν_{ee} into the equation for χ_e and using Eq. (44), we calculate that the total conduction heat flow at the transition layer is

$$Q_{T\text{-Cond}} = 5.8 \times 10^{-10} \cdot \frac{L_c\ [\text{m}] \cdot (T\ [\text{K}])^{5/2}}{\Lambda_{ee} \cdot D_a\ [\text{m}]}\ [\text{W/m}] \quad \text{and}$$
$$Q_{T\text{-Cond}} = 9 \times 10^{-10} \cdot \frac{L_c\ [\text{m}] \cdot (T\ [\text{K}])^{5/2}}{\Lambda_{ee}}\ [\text{W}] \tag{46}$$

where the first equation corresponds to slab geometry and the second one to a cylindrical capillary. In Eq. (46), we have dropped T_{wall}, because the plasma core temperature is usually much larger than the wall temperature or the characteristic temperature of the transition boundary region, Fig. 1. It should be stressed that Eq. (46) is an upper estimate for the radial heat flux.

In the model, we calculate the ratio of the radial thermal conduction heat flux, Eq. (46), to the radiation heat flux at the transition layer, the COND factor. When the COND factor becomes approximately one, thermal conduction becomes comparable to the radiation heat transfer and has to be taken into account in modeling capillary discharges. Because in our model we assume no thermal conduction, our model is valid only when the COND factor is much smaller than 1.

F. Plasma Composition and Geometry Assumptions

In our zero-dimensional model of ablative capillary discharge, we make the following plasma composition and geometry assumptions:

1) In the model, the capillary wall is polyethylene, C_4H_9. The radiation and plasma composition database has been constructed for this specific capillary wall composition and for a 4 mm slab capillary gap; we have used PrismSPECT to construct our database. The chosen wall composition and slab gap are not principal; similar databases can be constructed using PrismSPECT for other wall compositions and values of D_c.

2) The gas in the plasma core region is fully dissociated; this is valid for plasma temperatures larger than 0.7–1 eV.

3) As in [4,5,11–17,19,20], we neglect heat losses into the capillary wall, assuming that all radiation heat reaching the capillary wall is spent on its ablation.

4) The temperature of the ablative gas entering the plasma core region from the transition boundary layer, Fig. 1, is equal to T, the average temperature of the capillary plasma. In other words, the plasma radiation ablates the capillary wall, then dissociates and ionizes ablated gas, and finally heats it to the plasma temperature in the thin transition layer, as shown in Fig. 3. In this figure, a polyethylene molecule from the boiling capillary wall enters the transition layer (a) and becomes dissociated and ionized at the boundary between the transition layer and the plasma (b). This assumption has been made in all previous models [4,5,10–17,19,20] and, as discussed in Sec. I, can be verified only in a model that would include radiation heat transfer across the capillary; unfortunately, such a model does not exist yet. However, experimental observations [11,13] do not seem to contradict this assumption.

III. Description of the Model

A. Description of the Database

In our model, we use a radiation-plasma-composition database that has been constructed using PrismSPECT software. This software calculates the plasma composition and the radiative spectral flux to the "chamber walls" for a specified total number density of atoms (neutrals and ions), the element composition ratio (in our case, 4–9 for C_4H_9 capillary wall composition), plasma temperature, and geometry. Integrating the spectra over the frequency, we obtain the total radiation flux to the walls, F_{rad}, which we use in our database as well as plasma composition calculated by the PrismSPECT. Because PrismSPECT offers only two geometries, spherical and slab (no cylindrical geometry), we have selected slab geometry with a 4 mm slab gap. PrismSPECT assumes an infinite slab ($L_c = \infty$); therefore, applying the calculated radiation flux to the case of limited capillary length, Fig. 1, is correct when $L_c \gg D_c$.

Preliminary PrismSPECT calculations showed that, for a selected temperature range of 1–8 eV and the total number density of heavy particles between 10^{16}–10^{28} m^{-3}, only H_I, H_{II}, C_I, C_{II}, C_{III}, C_{IV}, and C_V (i.e. neutral atoms, ionized hydrogen, and singly up to four ionized carbon atoms) contribute to plasma composition; the number

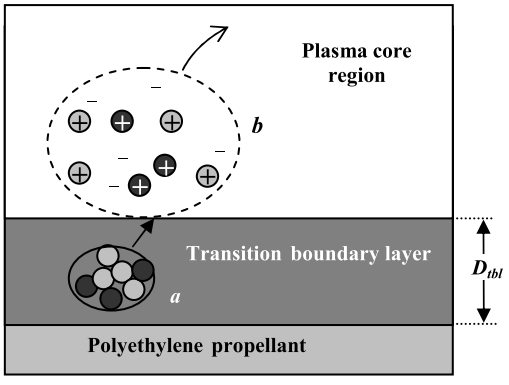

Fig. 3 Schematic of capillary discharge (not to scale) showing the transition boundary layer between the solid wall and the plasma.

densities of higher ionized carbon atom are negligibly small and are not included in the database.

It is worth noting that PrismSPECT includes free–free, free–bound, and bound–bound radiation and takes into account the pressure and Doppler broadenings of spectral lines and the reduction in ionization potential due to nonideal plasma effects.

Applying a standard linear-interpolation method to the database, we calculate the radiation flux and the plasma composition for a given plasma temperature and total number density of heavy particles (neutrals and ions).

B. Electrical Conductivity

Electrical conductivity plays a key role in the model by determining the rate of joule heating. Neglecting the induced magnetic field ($\beta \gg 1$), the electrical conductivity is given by

$$\sigma = \frac{n_e e^2}{m_e(\nu_{ei} + \nu_{ea})} \tag{47}$$

where the electron-neutral momentum transfer collision frequency ν_{ea} is given by Eq. (15), with the electron collision cross sections for neutral carbon and hydrogen atoms. For the electron–ion momentum transfer collision frequency ν_{ei}, we used the Spitzer equation [26] modified by Zollweg and Libermann [27] to account for nonideal effects:

$$\nu_{ei} = \frac{38 \cdot Z \cdot n_e \cdot e^2}{\gamma_e \cdot m_e \cdot T^{3/2}} \cdot \left(\frac{1}{2} \cdot \log[1 + 1.4 \cdot \Lambda_m^2]\right) \tag{48}$$

$$\Lambda_m = \frac{12 \cdot \pi \cdot \varepsilon_0 \cdot k_B \cdot T}{Z \cdot e^2} \cdot \left(\frac{\varepsilon_0 \cdot k_B \cdot T}{n_e \cdot e^2} + \left[\frac{3}{4 \cdot \pi \cdot n_i}\right]^{2/3}\right)^{1/2} \tag{49}$$

where $\varepsilon_0 = 8.854 \times 10^{-12}$ [F/m] is the permittivity of free space, and the factor $\gamma_e(Z)$ is a weak function of average ion charge Z and can be approximated as [13] $\gamma_e \approx 0.58 + 0.1 \cdot (Z - 1)$. It should be noted that Eq. (48) differs from Eq. (8) for ν_{ei}. However, for the case in which the nonideal effects are negligibly small, the plasma density is below 10^{24} m^{-3} and Eq. (48) converges to Eq. (8). Because for typical high-pressure capillary discharges the nonideal effects are rather small (differences in calculating ν_{ei} by Eqs. (8) and (48) are less than 30%), using Eq. (8) to calculate the LTE factor is acceptable. However, to calculate plasma resistance, we have to use the more accurate formula for ν_{ei}.

C. Equation for Ablation Rate of the Capillary Wall, Plasma Enthalpy

Calculating the enthalpy, h_{CH}, required to bring a "C_4H_9 polyethylene molecule" from the capillary wall to the plasma region, Fig. 3, is another key aspect of the model. Introducing the ablation rate of the capillary wall material as a number of "C_4H_9 molecules" coming into the capillary chamber per unit of time per unit of the slab length along the y axis, Fig. 1, we obtain

$$\dot{N}_{\mathrm{CH}}^{\mathrm{in}} = \frac{2 \cdot F_{\mathrm{rad}} \cdot L_c}{h_{\mathrm{CH}}} \tag{50}$$

where F_{rad} is the radiation flux at the transition boundary layer. The enthalpy is

$$h_{\mathrm{CH}} = \Delta\varepsilon_\Phi + c_p \cdot k_B \cdot T \cdot (1 + Z \cdot \varphi) \cdot (C_\alpha + H_\alpha) \tag{51}$$

where $C_\alpha = 4$; $H_\alpha = 9$ for a C_4H_9 polyethylene molecule; $\Delta\varepsilon_\Phi$ includes the energies of vaporization, dissociation, ionization, and electronic excitation; $c_P = \gamma/(\gamma - 1)$ is the specific heat at constant pressure with $\gamma = 5/3$; and $\varphi = n_i/(n_i + n_a)$ is the ionization ratio. The vaporization and dissociation energies are considered constants in the model and input parameters in the code. It is worth noting again that in the model we neglect the radiation heating of the bulk capillary wall, assuming that all radiation entering the transition layer is absorbed into this region and expended on the ablation of wall material, as stated in Eq. (50).

Calculating electronic excitation energy, we take into account 1) 16, 12, 6, 4, 1, 4, and 1 pseudolevels (i.e., groups of elementary levels with combined statistical degeneracy) and the average energy for $C_I, C_{II}, C_{III}, C_{IV}, C_V, H_I$, and H_{II}, respectively (the contributions of higher numbers of electron-partition functions into plasma enthalpy is negligibly small); and 2) the reduction in the ionization potentials due to the nonideality of the plasma. In nonideal plasmas the ionization potential decreases because in dense plasmas "free" electrons are no longer completely free (as in ideal plasmas) but remain weakly bound to the ions (not to the neutrals). Therefore, less energy is required to remove an electron to a weakly bond state (from which the electron can then easily escape, obtaining the necessary small amount of energy from elsewhere) than to a completely free state. The reduction in the ionization potential of an l-ionized atom [13,28–30] is

$$\Delta I_{l-)l+1} = \frac{l \cdot e^2}{4 \cdot \pi \cdot \varepsilon_0 \cdot (\lambda_D + \frac{\Omega}{8})} = \frac{l \cdot 1.44 \times 10^{-9}}{(\lambda_D + \frac{\Omega}{8})} \text{ [eV]} \tag{52}$$

where λ_D is the Debye length and Ω is the de Broglie wavelength:

$$\lambda_D = 6.9 \times 10^1 \cdot \left[\frac{T \text{ [K]}}{(1 + Z) \cdot n_e \text{ [m}^{-3}]}\right]^{1/2} \text{ [m]} \tag{53}$$

$$\Omega = \frac{h}{(2 \cdot \pi \cdot k_B \cdot m_e \cdot T)^{1/2}} = 7.45 \times 10^{-8} \cdot (T \text{ [K]})^{-1/2} \text{ [m]} \tag{54}$$

Here both the electron and positive-ion shielding are taken into account. For neutral atoms, l is equal to zero (they do not attract negative particles as well as positive ions), so there is no reduction in their ionization potentials. Substituting $n_e = 6 \times 10^{26}$ m^{-3}, $T =$ 4 eV, and $Z = 1$ into Eqs. (53) and (54), we obtain $\Delta I_{l \to l+1} \approx l \cdot 0.3$ eV. We would like to note that, because the Coulomb interaction is negative, the plasma pressure is also reduced because the electrons spend some time near ions not bombarding a "chamber wall." As has been shown [4,30], this reduction is less than 10% relative to the total plasma pressure for our conditions. Therefore, we neglect the pressure reduction in our model.

Thus, for a given plasma temperature and heavy particle number density we find the plasma composition and radiation flux at the transition layer, F_{rad}. Then, using the plasma composition, we calculate the average ion charge Z, the ionization energies while accounting for the reductions in the ionization potentials of heavy particles, the populations of the electron levels of carbon and hydrogen ionized and neutral atoms by employing the Saha equation, and, finally, $\Delta\varepsilon_\Phi$ and then h_{CH}. Substituting F_{rad} and h_{CH} into Eq. (50), we calculate the ablation rate of the wall material.

We have to stress that in Eq. (51) we have neglected the kinetic (nonthermal) energy of the ablated materials entering the plasma region. This is a correct assumption because the capillary length L_c is assumed to be much larger than the slab gap D_c, Fig. 1.

D. Mass and Energy Equations

An equation describing the outflow of ablated "polyethylene molecules" through the open capillary end, Fig. 1, can be written as

$$\dot{N}_{\mathrm{CH}}^{\mathrm{out}} = n_{\mathrm{CH,end}} \cdot D_c \cdot C_{s,\mathrm{end}} \tag{55}$$

with

$$C_{s,\mathrm{end}} = \left(\frac{\gamma \cdot P_{\mathrm{end}}}{\rho_{\mathrm{end}}}\right)^{1/2} = \left(\frac{\gamma \cdot (1 + Z_{\mathrm{end}} \cdot \varphi_{\mathrm{end}}) \cdot k_B \cdot T_{\mathrm{end}}}{\bar{M}}\right)^{1/2} \tag{56}$$

$$\bar{M} = \frac{C_\alpha \cdot M_{\mathrm{C}} + H_\alpha \cdot M_{\mathrm{H}}}{C_\alpha + H_\alpha} \tag{57}$$

where the index "end" denotes conditions at the exit plane and the absence of the index end denotes conditions averaged over the capillary volume in the "middle" of capillary. Here, n_{CH} is the mole number density of ablated molecules and M_C and M_H are the carbon and hydrogen atomic masses, respectively.

Combing Eqs. (50) and (55), using the isentropic flow relations [31] and assuming that the average ion charge and ionization ratio are preserved through the capillary up to the exit plane, $Z_{end} = Z$ and $\varphi_{end} = \varphi$, we obtain the following equation for the law of conservation of mass:

$$D_c \cdot L_c \cdot \frac{dn_{CH}}{dt} = \frac{2 \cdot F_{rad}(n_{CH}, T) \cdot L_c}{h_{CH}(n_{CH}, T)} - \Gamma \cdot n_{CH} \cdot D_c \cdot C_s \quad (58)$$

where

$$\Gamma = \left(\frac{2}{\gamma + 1}\right)^{\frac{\gamma+1}{2(\gamma+1)}} \quad (59)$$

Because we assume that there is no energy loss in the capillary discharge, we may conclude that all electrical energy put into the capillary discharge is leaving the capillary with the plasma jet at the exit plane or is expended on increasing the internal energy of the plasma inside the capillary. This gives the following equation for the law of conservation of energy:

$$D_c \cdot L_c \cdot \frac{d(n_{CH} \cdot \varepsilon_{CH})}{dt} = \frac{(J_{slab})^2 \cdot L_c}{D_c \cdot \sigma} - \Gamma \cdot n_{CH} \cdot D_c \cdot C_s \cdot h_{CH}(n_{CH}, T) \quad (60)$$

where ε_{CH} is the internal plasma energy,

$$h_{CH} - \varepsilon_{CH} = k_B \cdot T \quad (61)$$

Thus, solving Eqs. (58) and (60) for a given $J_{slab}(t)$ and initial plasma conditions, $n_{CH}(t = 0)$ and $T(t = 0)$, we obtain all characteristics of capillary discharge versus time. It has to be mentioned that the authors [5] used a similar system of equations for cylindrical capillaries to investigate the stability of the capillary discharge for the case of $J_{cyl} =$ const. and different initial plasma conditions. They also calculated the discharge parameters employing the resistor–inductor–capacitor circuit to self-consistently calculate the current and compared obtained results with experiments.

IV. Numerical Results

In the numerical results presented in this section, the energy of evaporation and dissociation were taken as zero (for polyethylene [11], they are much smaller than the ionization potentials of carbon and hydrogen and, because the ionization ratio of the plasma is larger than 15%, Fig. 4, they can be ignored). The capillary lengths were chosen as 4, 6, and 10 cm, and D_c was 4 mm. In this paper, we investigate the steady-state solutions of Eqs. (58) and (60). In our algorithm that solves Eqs. (58) and (60) with the left-hand sides equal to zero, the plasma temperature T is an input parameter. Given T, solving Eq. (58), we obtain the mole number density of ablated molecules in the plasma core, n_{CH}. Then, substituting T and the calculated n_{CH} into Eq. (60) we obtain J_{slab}, the required discharge current to maintain the plasma temperature equal to T.

As shown in Figs. 4–10, the model gives two solutions at a given plasma temperature. The first solution corresponds to a regime in which the plasma is so dense that the radiation mean free path λ_{rad} is smaller than or equal to the capillary gap, the case of SHP capillary discharge, solid curves in Figs. 4–10. The second regime, dashed curves, corresponds to the case in which the plasma density is much lower such that λ_{rad} is much larger than D_c, that is, the case of MHP capillary discharge. As shown in Figs. 4–10, the regimes converge at a small plasma temperature, and there are no steady-state solutions for plasma temperatures smaller than 1.215, 1.43, and 1.74 for $L_c = 4$, 6, and 10 cm, respectively. In the SHP regime, the pressure is much larger than in the MHP regime, Fig. 5; therefore, the ionization

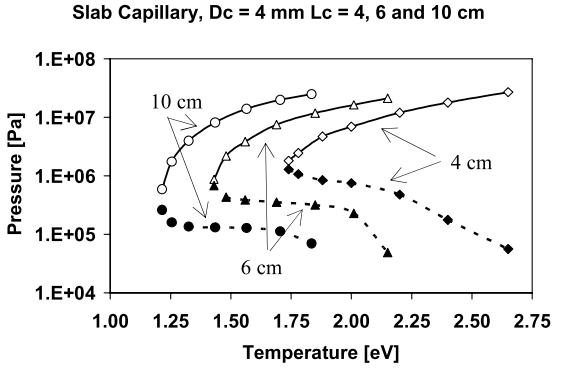

Fig. 5 Plasma pressure; dashed line: MHP regime, solid line: SHP regime.

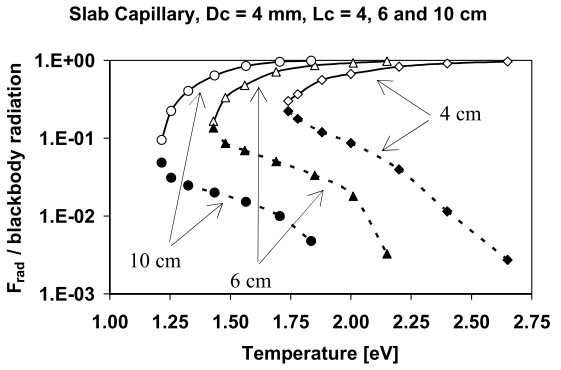

Fig. 6 F_{rad}/F_{BBR}; dashed line: MHP regime, solid line: SHP regime.

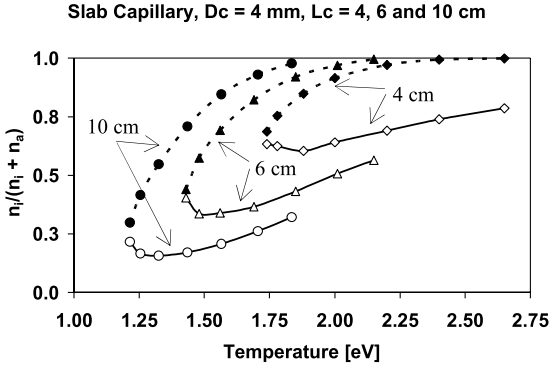

Fig. 4 Ionization ratio; dashed line: MHP regime, solid line: SHP regime.

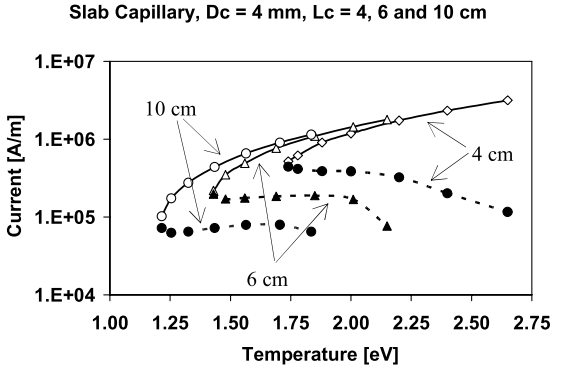

Fig. 7 Discharge current; dashed line: MHP regime, solid line: SHP regime.

ratio is larger for the SHP regime than for the MHP regime at the same plasma temperature, Fig. 4.

Figure 6 shows the ratio of radiation flux at the transition layer, Fig. 1, to the blackbody radiation flux with the same plasma temperature. As one can see, the gray factor f, Eq. (3), varies from 0.1 to almost 1 for the SHP regime and from 0.23 to 0.03 for the MHP regime depending on the plasma temperature and capillary length. This indicates that the gray factor can change noticeably with time in a nonsteady operation regime; therefore, assuming that it is constant (as has been done in models [11–17,19,20]) can lead to false results. The current, power, and capillary wall ablation rate per 1 m of capillary length in the y direction are shown in Figs. 7–9. As one can see, the parameters of capillary discharges may differ by more than 1 order of magnitude or even as much as 2 orders for the SHP and MHP regimes.

Figures 10–15 show the dependence of the LTE factor, β, recombination LPCE factor, ionization LPCE factor, COND factors,

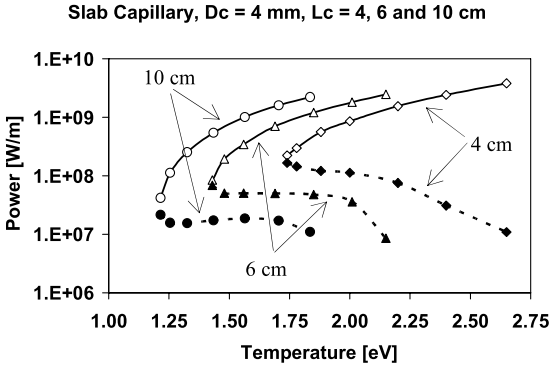

Fig. 8 Discharge power; dashed line: MHP regime, solid line: SHP regime.

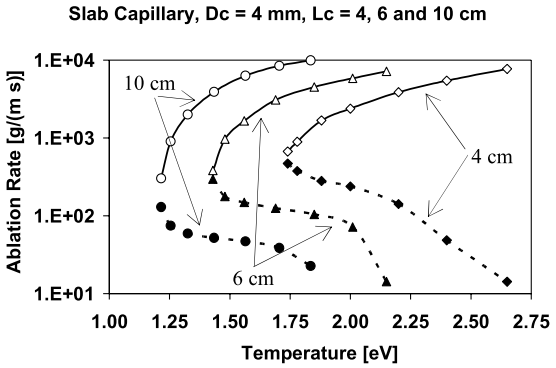

Fig. 9 Ablation rate; dashed line: MHP regime, solid line: SHP regime.

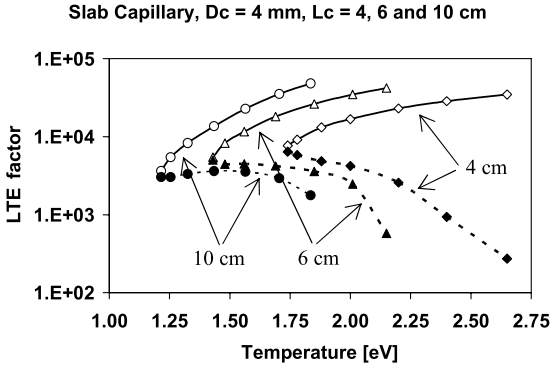

Fig. 10 LTE factor; dashed line: MHP regime, solid line: SHP regime.

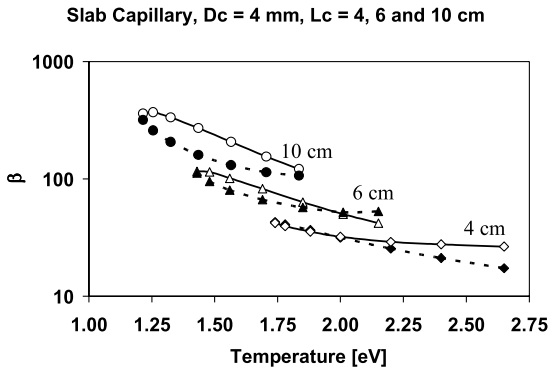

Fig. 11 β factor; dashed line: MHP regime, solid line: SHP regime.

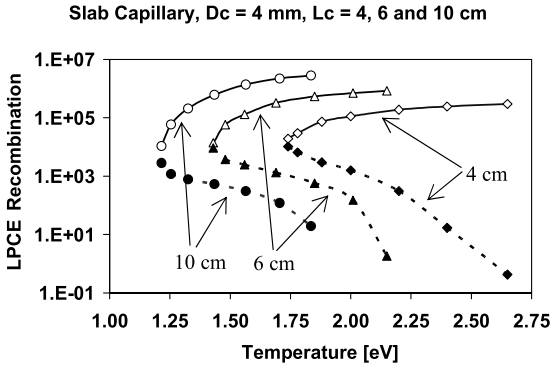

Fig. 12 LPCE factor; dashed line: MHP regime, solid line: SHP regime.

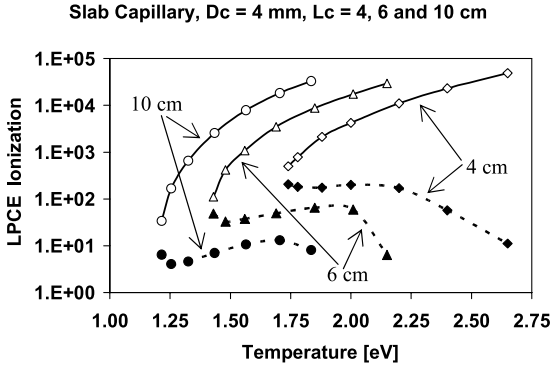

Fig. 13 LPCE factor; dashed line: MHP regime, solid line: SHP regime.

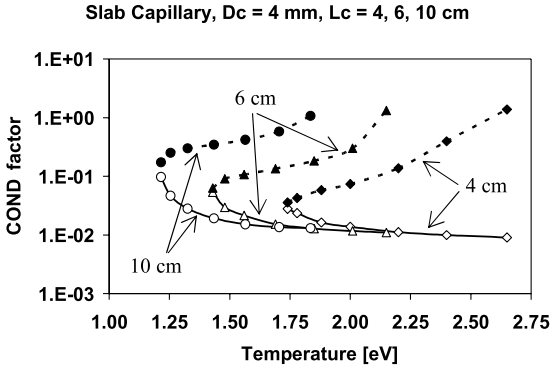

Fig. 14 COND factor; dashed line: MHP regime, solid line: SHP regime.

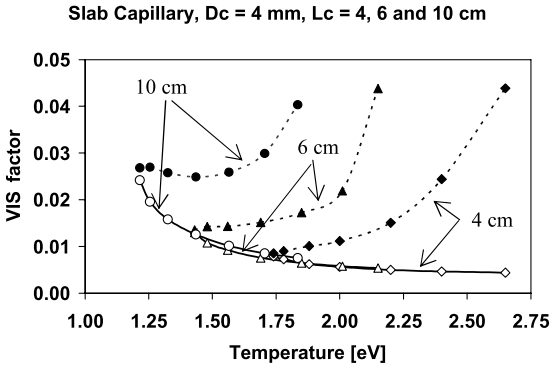

Fig. 15 VIS factor; dashed line: MHP regime, solid line: SHP regime.

and VIS factor versus temperature for both regimes. As one can see, the SHP regime satisfies all five assumptions of the model: the LTE factor, β, and both LPCE factors are much larger than 1, and the COND and VIS factors are much smaller than 1 in all temperature regions. However, the MHP regime satisfies only three of the model assumptions in all temperature regions: the LTE factor and β are much larger than 1 and the VIS factor is much smaller than 1, whereas the COND factor in this regime increases with temperature and becomes larger than 1 and the total LPCE factor (which is the smallest factor of recombination and ionization factors) decreases and becomes smaller than 1, Figs. 12 and 14.

Thus, the presented model cannot adequately describe the MHP regime for the case of relatively high temperatures, when the thermal heat conduction becomes larger than radiation heat flux at the transition layer, and the Saha equilibrium cannot be applied to determine the plasma composition. However, because in this regime the calculated LTE factor and β are both much larger than 1 even when the COND and LPCE factors are approximately 1, we may conclude that, even for the case in which thermal conduction is much larger than radiation (heat transfer of the ablative capillary discharge is controlled by thermal conductivity and not by radiation) and plasma composition cannot be described by the Saha equation (plasma composition is determined by kinetic processes and not by thermodynamic equilibrium), the capillary discharge can be operated at conditions when the LTE factor and β are much larger than 1. This operating regime may be attractive for thruster applications as well as for SHP or MHP regimes, depending on specific applications.

V. Conclusions

We present a zero-dimensional time-dependent high-pressure slab capillary discharge model that, for the first time, includes a heat-transfer radiation model based on a radiation database to self-consistently calculate the radiation heat flux at the thin transition boundary layer between the uniform plasma core and the ablative capillary walls. We also provide a detailed analysis of the assumptions made in the model. The model predicts the existence of two steady-state capillary discharge regimes, the superhigh-pressure regime ($\gamma_{\text{rad}<D_c}$) and the moderately high-pressure regime ($\gamma_{\text{rad}} > D_c$). Both regimes converge at the small plasma temperature, and there is no steady-state solution for smaller plasma temperatures. Both operating regimes may be attractive for thruster applications, depending on specific applications. It should be stressed that future investigation of the stability of steady-state SHP and MHP regimes is important, and we are planning to address this issue in the future. The model also allows the calculation of the grey factor, the ratio of radiation flux at the transition boundary layer to the blackbody radiation flux with the same plasma temperature. As shown, the grey factor may vary from 0.02 to almost 1 depending on the plasma parameters and capillary geometry. Thus, the assumption that the grey factor is constant in a nonsteady operation regime (as in models [11–17,19,20]) can lead to false results.

Acknowledgments

The author thanks J.-L. Cambier for helpful discussion during the course of the research for this paper and would like to express his gratitude to A. Pekker and M. Kapper for their kind help in preparing the text of this paper.

References

[1] Burton, R. L., Goldstein, S. A., Tidman, D. A., and Winsor, N. K., "Theory of the Pulsed Electrothermal Thruster," AIAA Paper 1982-1952, Nov. 1982.

[2] Burton, R. L., Goldstein, S. A., Hilko, B. K., Tidman, D. A., and Winsor, N. K., "Investigation of a Pulsed Electrothermal Thruster," GT Devices, Inc., NASA-CR-168266, Alexandria, VA, Oct. 1983.

[3] Burton, R. L., Goldstein, S. A., Hilko, B. K., Tidman, D. A., and Winsor, N. K., "Experimental Investigation of the Pulsed Electrothermal (PET) Thruster," , AIAA Paper 1984-1386, June 1984.

[4] Pekker, L., and Cambier, J.-L., "A Model of Ablative Capillary Discharge," *13th International Heat Transfer Conference*, Begell House, Inc., Redding, CT, Aug. 2006. doi:10.1615/IHTC13.p4.80

[5] Cambier, J.-L., Young, M., Pekker, L., and Pancotti, A., "Capillary Discharge Based Pulsed Plasma Thruster," *30th International Electrical Propulsion Conference*, 2007-238, 2007.

[6] Keidar, M., Boyd, I. D., and Beilis, I. I., "Electrical Discharge in the Teflon Cavity of a Coaxial Pulsed Plasma Thruster," *IEEE Transactions on Plasma Science*, Vol. 28, No. 2, 2000, pp. 376–385. doi:10.1109/27.848096

[7] Keidar, M., and Boyd, I. D., "Model of an Electrothermal Pulsed Plasma Thruster," *Journal of Propulsion and Power*, Vol. 19, No. 3, 2003, pp. 424–430. doi:10.2514/2.6125

[8] Keidar, M., and Boyd, I. D., "Ablation Study in the Capillary Discharge of an Electrothermal Gun," *Journal of Applied Physics*, Vol. 99, No. 5 2006, pp. 053301.1–053301.7. doi:10.1063/1.2174111

[9] Edamitsu, T., and Tahara, H., "Experimental and Numerical Study of an Electrothermal Pulsed Thruster for Small Satellites," *Vacuum*, Vol. 80, No. 11–12, 2006, pp. 1223–1228. doi:10.1016/j.vacuum.2006.01.055

[10] Tidman, D. A., Y. Thio, Y. C., Goldstein, S. A., and Spicer, D. S., "High Velocity Electrothermal Mass Launchers," GT Devices, Inc., GTD 86-7, Alexandria, VA, 1986.

[11] Loeb, A., and Kaplan, Z., "A Theoretical Model for the Physical Processes in the Confined High Pressure Discharges of Electrothermal Launchers," *IEEE Transactions on Magnetics*, Vol. 25, No. 1, 1989, pp. 342–346. doi:10.1109/20.22561

[12] Gilligan, J. G., and Mohanti, R. B., "Time-Dependent Numerical Simulation of Ablation-Controlled Arcs," *IEEE Transactions on Plasma Science*, Vol. 18, No. 2, 1990, pp. 190–197. doi:10.1109/27.131019

[13] Powell, J. D., and Zielinski, A. E., "Theory and Experiment for an Ablative-Capillary Discharge and Application to Electrothermal-Chemical Guns," U.S. Army Ballistic Research Lab. Rept. BRL-TR-3355, Aberdeen Proving Ground, MD, June 1992.

[14] Powell, J. D., and Zielinski, A. E., "Capillary Discharge in the Electrothermal Gun," *IEEE Transactions on Magnetics*, Vol. 29, No. 1, 1993, pp. 591–596. doi:10.1109/20.195642

[15] Zoler, D., Saphier, D., and Alimi, R., "A Numerical Study of the Evolution of Plasma Parameters in an Ablative Capillary Discharge for a Two-Pulse Form of Energy Input," *Journal of Physics D: Applied Physics*, Vol. 27, No. 7, 1994, pp. 1423–1432. doi:10.1088/0022-3727/27/7/013

[16] Zoler, D., and Alimi, R., "A Proof of the Need for Consistent Treatment in Modeling of Capillary Ablative Discharges," *Journal of Physics D: Applied Physics*, Vol. 28, No. 6, 1995, pp. 1141–1152. doi:10.1088/0022-3727/28/6/017

[17] Raja, L. L., Varghese, P. L., and Wilson, D. E., "Modeling of the Electrogun Metal Vapor Plasma Discharge," *Journal of Thermophysics and Heat Transfer*, Vol. 11, No. 3, 1997, pp. 353–360. doi:10.2514/2.6273

[18] Shafir, N., Zoler, D., Wald, S., and Shapiro, M., "Reliable, High Reproducible Plasma Injectors for Electrothermal and Electrothermal-Chemical Launcher," *IEEE Transactions on Magnetics*, Vol. 41, No. 1, 2005, pp. 355–359. doi:10.1109/TMAG.2004.839275

[19] Kim, K., "Time-Dependent One-Dimensional Modeling of Pulsed Plasma Discharge in a Capillary Plasma Device," *IEEE Transactions on Plasma Science*, Vol. 31, No. 4, 2003, pp. 729–735. doi:10.1109/TPS.2003.815472

[20] Kim, K., "Numerical Simulation of Capillary Plasma Flow Generated by High-Current Pulsed Power," *International Journal of Thermal Sciences*, Vol. 44, No. 11, 2005, pp. 1039–1046. doi:10.1016/j.ijthermalsci.2005.04.007

[21] Cros, B., Courtois, C., Malka, G., Matthieussent, G., and Marques, J. R., Dorchies, F., Amiranoff, F., Rebibo, S., Hamoniaux, G., Blanchot, N., and Miquel, J.L., "Extending Plasma Accelerators: Guiding with Capillary Tubes," *IEEE Transactions on Plasma Science*, Vol. 28, No. 4, 2000, pp. 1071–1077. doi:10.1109/27.893291

[22] Bobrova, N. A., Esaulov, A. A., Sakai, J.-I., Sasorov, P. V., Spence, D. J., Butler, A., Hooker, S.M., and Bulanov, S. V., "Simulation of Hydrogen-Filled Capillary Discharge Waveguide," *Physical Review E (Statistical Physics, Plasmas, Fluids, and Related Interdisciplinary Topics)*, Vol. 65, No. 1, 2001. doi:10.1103/PhysRevE.65.016407

[23] Spence, D. J., Bulter, A., and Hooker, S. M., "Gas-Filled Capillary Discharge Waveguides," *Journal of the Optical Society of America B (Optical Physics)*, Vol. 20, No. 1, 2003, pp. 138–151. doi:10.1364/JOSAB.20.000138

[24] Mocek, T., McKenna, C. M., Cros, B., Sebban, S., and Spence, D. J., Maynard, G., Bettaibi, I., Vorontsov, V., Gonsavles, A. J., and Hooker, S. M., "Dramatic Enhancement of xuv Laser Output Using a Multimode Gas-Filled Capillary Waveguide," *Physical Review A*, Vol. 71, No. 1, 2005. doi:10.1103/PhysRevA.71.013804

[25] Raizer, Y. P., "Gas Discharge Physics," Springer, New York, 1997.

[26] Spitzer, L., "Physics of Fully Ionized Gases", Interscience, New York, 1953, Chap. 5.

[27] Zollweg, R. J., and Liebermann, R. W., "Electrical Conductivity of Nonideal Plasmas," *Journal of Applied Physics*, Vol. 62, No. 9, 1987, 1987, pp. 3621–3637. doi:10.1063/1.339265

[28] Ebeling, W., and Sandig, R., "Theory of the Ionization Equilibrium in Dense Plasmas," *Annalen der Physik (Berlin)*, Vol. 483, No. 4, 1973, pp. 289–305. doi:10.1002/andp.19734830402

[29] Ebeling, W., Foster, A., Hess, H., and Romanovsky, M. Yu, "Thermodynamic and Kinetic of Hot Nonideal Plasmas," *Plasma Physics and Controlled Fusion*, Vol. 38, No. 12A, 1996, pp. A31–A47. doi:10.1088/0741-3335/38/12A/004

[30] Griem, R. H., "High-Density Corrections in Plasma Spectroscopy," *Physical Review*, Vol. 128, No. 3, 1962, pp. 997–1003. doi:10.1103/PhysRev.128.997

[31] Emanuel, G., "Gasdynamics: Theory and Applications," AIAA Education Series, AIAA, New York, 1986

A. Gallimore
Associate Editor